applied sciences

MDPI

Article

Impact of Nonlinear Thermal Radiation on MHD Nanofluid Thin Film Flow over a Horizontally Rotating Disk

Zahir Shah [1], Abdullah Dawar [2], Poom Kumam [3,4,5,*], Waris Khan [6] and Saeed Islam [1]

1 Department of Mathematics, Abdul Wali Khan University, Mardan 23200, Pakistan; Zahir1987@yahoo.com (Z.S.); saeedislam@awkum.edu.pk (S.I.)
2 Department of Mathematics, Qurtuba University of Science and Information Technology, Peshawar 25000, Pakistan; abdullah.mathematician@gmail.com
3 KMUTT-Fixed Point Research Laboratory, Room SCL 802 Fixed Point Laboratory, Science Laboratory Building, Department of Mathematics, Faculty of Science, King Mongkut's University of Technology Thonburi (KMUTT), 126 Pracha-Uthit Road, Bang Mod, Thrung Khru, Bangkok 10140, Thailand
4 KMUTT-Fixed Point Theory and Applications Research Group, Theoretical and Computational Science Center (TaCS), Science Laboratory Building, Faculty of Science, King Mongkut's University of Technology Thonburi (KMUTT), 126 Pracha-Uthit Road, Bang Mod, Thrung Khru, Bangkok 10140, Thailand
5 Department of Medical Research, China Medical University Hospital, China Medical University, Taichung 40402, Taiwan
6 Department of Mathematics, Kohat University of Science and technology, Kohat 26000, Pakistan; Wariskhan758@yahoo.com
* Correspondence: poom.kum@kmutt.ac.th; Tel.: +66-2-4708-994

Received: 22 February 2019; Accepted: 8 April 2019; Published: 12 April 2019

check for updates

Abstract: Nanoscience can be stated as a superlative way of changing the properties of a working fluid. Heat transmission features during the flow of nanofluids are an imperative rule from the industrial and technological point of view. This article presents a thin film flow of viscous nanofluids over a horizontal rotating disk. The impact of non-linear thermal radiation and a uniform magnetic field is emphasized in this work. The governing equations were transformed and solved by the homotopy analysis method and the ND-Solve technique. Both analytical and numerical results are compared graphically and numerically, and excellent agreement was obtained. Skin friction and the Nusselt number were calculated numerically. It is concluded that the thin film thickness of nanofluids reduces with enhanced values of the magnetic parameter. In addition, the nanofluid temperature was augmented with increasing values of the thermal radiation parameter. The impact of emerging parameters on velocities and temperature profiles were obtainable through graphs and were deliberated on in detail.

Keywords: nanofluids; heat transfer; thin film; nonlinear radiation; MHD; numerical approach

1. Introduction

Over the last few years, researchers have given prodigious attention to thin film flows. The elementary impression behind such a significant thought is the applications and mechanism of it. The investigation of thin film flow has had important commitment because of its vast applications and uses in engineering, technology, and industries. Cable, fibber undercoat, striating of foodstuff, extrusion of metal and polymer, constant forming, fluidization of the device, elastic sheets drawing, chemical treating tools, and exchanges are several uses. In surveying these applications, our attention was drawn to cultivating the examination of liquid film on a stretching surface. The first theoretical analysis on liquid film flow was done by Emslie et al. [1]. During the disk rotating process, the balance between centrifugal and viscous forces was considered in this examination. They simplified the Navier–Stokes equations and concluded that the film is uniformly maintained with its continuous thinning property. Higgins [2] considered the influence of film inertia over a rotating disk. The liquid film over a rotating plate with constant angular velocity was analyzed by Dorfman [3]. The fluid film rotation from an accelerating disk was analyzed by Wang et al. [4]. For the thin and thick film parameter and the small accelerating parameter, the asymptotic solutions were obtained. Andersson et al. [5] asymptotically and numerically examined the magnetohydrodynamics (MHD) liquid thin film due to a rotating disk. Over a rotating disk, Dandapat and Singh [6] examined the two layer film flow. The heat transfer flow of thin film flows of nanofluids has been deliberated by Sandeep et al. [7]. The movement of a finite thin liquid over a stretched sheet was scrutinized by Usha et al. [8]. Khan et al. [9] studied the nanofluid film flow of Eyring-Powell with graphene nanoparticles. The recent study of nanofluid flow of non-Newtonian fluids using different models in different geometries can be seen in [10–12]. Jawad et al. [13,14] investigated magneto hydrodynamic nanofluid thin film flow with the joule and slip effect. Under the influence of slip velocity, Megahe [15] examined the Casson fluid flow over a stretched surface. The thin film flow with a new modification was deliberated by Khan et al. [16] and Tahir et al. [17].

With the advent of nanoscience; nanofluids have turned into a focal point of consideration in the investigation of nanofluid flow in the presence of nanoparticles. Nanofluids are arranged by scattering 10^9 nm-sized substances, such as nanoparticles, nanotubes, nanofibers, droplets, etc., in fluids. Actually, nanofluids are nanoscale shattered suspensions involving concise nanometer sized materials. These are two-period systems; the first one is the solid phase and the second one is the liquid phase. Nanofluids must be utilized to augment the thermal conductivity of the fluids and can be more stable with better mixing. Nano science is used to find the appropriate working fluid to reach convective heat transfer enhancement.

Nanofluids are used in microelectronics, hybrid powered engines, pharmaceutical procedures, fuel cells, and nanotechnologies. In view of their importance, Sheikholeslami et al. [18–22] investigated nanofluid flow and presented its applications. The flow of nanofluid over a stretched surface has been determined by Abolbashari et al. [20]. The Maxwell nanofluid flow has been presented by Hayat et al. [21]. The mixed convection flow of MHD Erying–Powell fluid has been inspected by Malik et al. [22]. The flow of Maxwell fluid over a vertical stretched surface has been examined by Nadeem et al. [23]. With convective heat and mass transfer, the MHD non-Newtonian fluid through a cone has been probed by Raju et al. [24]. The flow of nanofluids with heat transfer over a plate has been examined by Rokni et al. [25]. The numerical investigation of non-Newtonian fluid flow over a stretched surface has been observed by Nadeem et al. [26]. The MHD flow of Jeffrey nanofluids with convective boundary conditions has been examined by Shehzad et al. [27]. With heat transfer, the MHD flow of nanoliquids has been determined by Sheiholeslami et al. [28].

In order to manipulate mechanical and/or thermal energy in electrically conducting polymers, magnetic fields play a significant cost saving role. The natural heat transfer process due to temperature differences within a body or between two bodies at different temperatures is best analyzed by the use of MHD. MHD also has various practical applications in industrial and environmental sciences. Shah et al. [29–34] investigated MHD heat transfer nanofluids with microstructure properties that have different aspects in different geometries. Hammed et al. [35] investigated the electric and magnetic impact on Maxwell nanofluids. Dawar et al. [36] studied squeezing MHD carbon nanotube nanofluids. The other relevant studies can be seen in [37–40]. The most recent study on nanofluids and nanotubes with thermal conductivity can be seen in [41–50].

The above mentioned literature survey has surpassed previous studies. Now we are in position to study the thin film flow of viscous nanofluids over a horizontal rotating disk. The impact of non-linear thermal radiation and uniform magnetic field are emphasized in this work. The governing equations have been solved by using the homotopy analysis method and the ND-Solve technique. The impact of non-linear thermal radiation and uniform magnetic fields are emphasized in this work.

2. Mathematical Formulation

If the unsteady magnetohydrodynamic flow is assumed, heat and mass transfer nanofluids flow in a thin finite liquid film over a stretching rotating disk. The thin elastic disk emerges radially from a narrow slit at the origin of the cylindrical coordinate system (r, φ, z). The scheme of the formulated problem is shown in Figure 1.

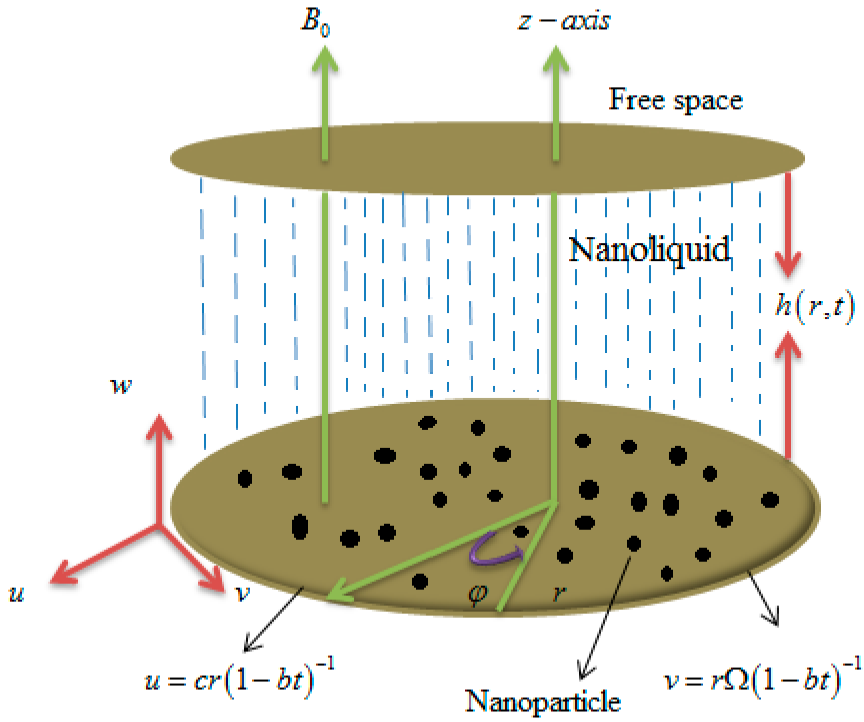

Figure 1. Physical sketch of the problem.

The time dependent stretching velocity is written as

$$u = cr(1 - bt)^{-1}, \tag{1}$$

Here c and b represent the stretching parameter and positive constant respectively. The time dependent disk rotating velocity is written as

$$v = r\Omega(1 - bt)^{-1}, \tag{2}$$

where Ω is the rotating rate of the disk. The stretchable rotating disk surface temperature T_s is defined as

$$T_s = T_0 - T_{ref}\frac{\Omega r^2}{\nu_{nf}(1 - bt)^{1.5}}, \tag{3}$$

Here T_0 and T_{ref} represent temperature at the origin and a constant reference temperature, respectively. The magnetic field is applied along the z-direction which is defined as

$$B(t) = B_0(1 - bt)^{-0.5}, \tag{4}$$

The concentration at the disk surface C_s varying with distance r is written as

$$C_s = C_0 - C_{ref}\frac{\Omega r^2}{\nu_{nf}(1-bt)^{1.5}}, \tag{5}$$

Here, C_0 and C_{ref} represent the concentration at the origin and reference concentration, respectively.

Using the above suppositions, and boundary conditions, the governing equations of the flow problem are

$$\frac{\partial u}{\partial t} + \frac{u}{r} + \frac{\partial w}{\partial z} = 0, \tag{6}$$

$$\frac{\partial u}{\partial t} + \frac{\partial u}{\partial r} + w\frac{\partial u}{\partial z} - \frac{v^2}{r} = \nu_{nf}\left(\frac{\partial^2 u}{\partial z^2}\right) - \frac{\sigma_{nf}B_0^2}{\rho_{nf}(1-bt)}u, \tag{7}$$

$$\frac{\partial v}{\partial t} + \frac{\partial v}{\partial r} + w\frac{\partial v}{\partial z} + \frac{uv}{r} = \nu_{nf}\left(\frac{\partial^2 v}{\partial z^2}\right) - \frac{\sigma_{nf}B_0^2}{\rho_{nf}(1-bt)}v, \tag{8}$$

$$\frac{\partial T}{\partial t} + u\frac{\partial T}{\partial r} + w\frac{\partial T}{\partial z} = \alpha_{nf}\left(\frac{\partial^2 T}{\partial z^2}\right) + \frac{16\sigma^*}{3\rho c_p k^*}\frac{\partial}{\partial z}\left(T^3\frac{\partial T}{\partial z}\right), \tag{9}$$

Here $u,\ v$ and w are the velocity components in their respective directions as shown in Figure 1. Also $\sigma^*, k^*, \nu_{nf}, \sigma_{nf}, \rho_{nf}, \left(\rho C_p\right)_{nf}, \alpha_{nf}$ are the Stephan–Boltzmann constant, mean absorption coefficient, kinematic viscosity, electrical conductivity, density, heat capacity and thermal diffusivity which are defined as

$$\begin{gathered}
\sigma_{nf} = 1 + \frac{3\left(\sigma_s/\sigma_f - 1\right)\phi}{\left(\sigma_s/\sigma_f + 2\right) - \left(\sigma_s/\sigma_f - 1\right)\phi}\sigma_f, \qquad \rho_{nf} = (1-\phi)\rho_f + \phi\rho_s, \\
\left(\rho C_p\right)_{nf} = (1-\phi)\left(\rho C_p\right)_f + \phi\left(\rho C_p\right)_s, \qquad \frac{k_{nf}}{k_f} = \frac{k_s + 2k_f - 2\phi\left(k_f - k_s\right)}{k_s + 2k_f + 2\phi\left(k_f - k_s\right)}, \\
\alpha_{nf} = \frac{k_{nf}}{\left(\rho c_p\right)_{nf}}.
\end{gathered} \tag{10}$$

The respective boundary conditions are

$$\begin{gathered}
u = cr(1-bt)^{-0.5}, v = r\Omega(1-bt)^{-0.5}, w = 0, T = T_s \quad at \quad z = 0, \\
\frac{\partial u}{\partial z} = \frac{\partial v}{\partial z} = 0, \quad w = \frac{\partial h}{\partial t} + u\frac{\partial h}{\partial r}, \quad \frac{\partial T}{\partial z} = 0 \quad at \quad z = h.
\end{gathered} \tag{11}$$

The correspondence variables are defined as

$$\begin{gathered}
u = \frac{r\Omega}{(1-bt)^{0.5}}f'(\eta), v = \frac{r\Omega}{(1-bt)^{0.5}}g(\eta), w = -2\left(\nu\Omega/(1-bt)\right)^{0.5}f(\eta), \\
h(t) = \left(\frac{\nu}{\Omega}(1-bt)\right)^{0.5}\beta, T = T_0 - T_{ref}\frac{\Omega r^2}{\nu(1-bt)^{1.5}}\theta(\eta), \eta = \left(\Omega/\nu(1-bt)\right)^{0.5}z.
\end{gathered} \tag{12}$$

Substituting Equation (12) in Equations (7)–(9), the following system of equations is achieved

$$f''' - S\left(f' + \frac{\eta}{2}f''\right) - \left(f'^2 - g^2 - 2ff''\right) - \left(\frac{\varepsilon_1}{\varepsilon_2}\right)Mf' = 0, \tag{13}$$

$$g'' - S\left(g + \frac{\eta}{2}g'\right) - 2(f'g + fg') - \left(\frac{\varepsilon_1}{\varepsilon_2}\right)Mg = 0, \tag{14}$$

$$\begin{gathered}
\left(1 + \frac{4}{3}Rd\right)\theta'' + \frac{4}{3}Rd\left(\frac{\varepsilon_3}{\varepsilon_1}\right)\begin{bmatrix} (\theta_w - 1)^3\left(3\theta^2\theta'^2 + \theta^3\theta''\right) + \\ 3(\theta_w - 1)^2\left(2\theta\theta'^2 + \theta^2\theta''\right) + \\ 3(\theta_w - 1)\left(\theta'^2 + \theta\theta''\right) \end{bmatrix} \\
+ 2\Pr(f\theta' - f'\theta) - \frac{1}{2}\Pr S(\eta\theta' + 3\theta) = 0,
\end{gathered} \tag{15}$$

With transformed boundary conditions

$$\begin{aligned} &f(0)=0, f'(0)=\omega, g(0)=1, \theta(0)=1, \\ &f(\beta)=\tfrac{S\beta}{4}, f''(\beta)=0, g''(\beta)=0, \theta'(\beta)=0. \end{aligned} \quad (16)$$

In Equations (13)–(15), $S=\frac{b}{\Omega}$ is a measure of unsteadiness, $M=\frac{B_0^2}{\Omega(1-bt)}$ signifies the magnetic parameter, $\Pr=\frac{\nu}{b}$ indicates the Prandtl number, $\theta_w=\frac{T_s}{T_0}$ represents the temperature ration parameter, $Rd=\frac{4\sigma^* T_0^3}{kk^*}$ indicates the radiation parameter, $\omega=\frac{c}{\Omega}$ represents the rotation parameter, and $\beta=\left(\frac{\nu}{\Omega(1-bt)}\right)^{0.5} h$ specifies the value of similarity variable at free space. Finally, ε_1, ε_2 and ε_3 are constants defined in the following way

$$\begin{aligned} &\varepsilon_1=(1-\phi)\rho_f+\phi\rho_s, \\ &\varepsilon_2=\frac{3\left(\sigma_s/\sigma_f-1\right)\phi}{\left(\sigma_s/\sigma_f+2\right)-\left(\sigma_s/\sigma_f-1\right)\phi}\sigma_f, \\ &\varepsilon_3=\frac{k_s+2k_f-2\phi\left(k_f-k_s\right)}{k_s+2k_f+2\phi\left(k_f-k_s\right)}. \end{aligned} \quad (17)$$

The skin friction coefficient and local Nusselt number are defined as

$$\mathrm{Re}^{-1/2} Cf_r = f''(0), \quad (18)$$

$$\mathrm{Re}^{-1/2} Nu_r = -\left\{1+\frac{4}{3}Rd\left(1+(\theta_w-1)\theta(0)\right)^3\right\}\theta'(0), \quad (19)$$

where $\mathrm{Re}^{1/2}=r\sqrt{\frac{c}{v}}$ is the local Reynolds number.

3. Solution Procedure

For a solution of the modeled Equations (13)–(15) with boundary conditions (16) are solved with the homotopy analysis method (HAM) [44–50]. HAM is used due to its outstanding outcomes. The preliminary guesses are selected as follows:

$$f_0(f)=\eta,\ g_0(g)=1,\ \theta_0(\theta)=1. \quad (20)$$

The linear operators are denoted as L_f, L_g and L_θ are represented as

$$L_f(f)=f_{\eta\eta\eta},\ L_g(g)=g_{\eta\eta},\ L_\theta\big(\theta\big)=\theta_{\eta\eta}. \quad (21)$$

which has the following applicability:

$$L_f(C_1+C_2\eta+C_3\eta^2+C_4\eta^3)=0, L_g(C_5+C_6\eta+C_7\eta^2)=0, L_\theta(C_8+C_9\eta)=0. \quad (22)$$

where $C_i(i=1,2,3,\ldots 9)$ are constant.

Regrettably there are many practical systems that lead to an analytical solution, and analytical solutions are of limited use. That is why we use the numerical approach to make an answer close to the practical result. Those solutions which cannot be used in complete mathematical expressions are numerical solutions. There are almost no problems in nature that are exactly solvable, which creates a problem. However, there are about three or four of these problems in nature that have already been solved but unfortunately even numerical methods cannot give an exact solution. Numerical techniques can handle any completed physical geometries which are often impossible to solve analytically. Figures 2–4 show the comparison of the HAM and ND-Solve technique for velocities and temperature functions. Figure 5 shows the total residual error for velocity and temperature functions. Tables 1–4 represent the comparison of the HAM and ND-Solve technique for velocity and temperature functions. From these tables, an excellent agreement between HAM and numerical (ND-Solve) techniques are obtained. Table 5 demonstrates the individual residual square errors for velocities and temperature functions. A fast convergence of the solutions is observed in Table 5. Table 4 represents the individual residual square errors for velocity $f'(\eta)$, $g(\eta)$ and $\theta(\eta)$.

Table 1. The comparison of HAM and ND-Solve for different values of the dimensionless variable η.

η	HAM Solution	ND-Solution	Absolute Error
0.0	0.000000	3.245990×10^{-9}	3.245990×10^{-9}
0.2	0.185094	0.185094	1.205310×10^{-7}
0.4	0.344936	0.344935	4.805570×10^{-7}
0.6	0.486721	0.486720	1.053600×10^{-6}
0.8	0.617341	0.617339	1.733100×10^{-6}
1.0	0.742857	0.742855	2.627600×10^{-6}

Table 2. Comparison of HAM and ND-Solve for velocity function $f'(\eta)$ w.r.t. different values of the dimensionless variable η.

η	HAM Solution	ND Solution	Absolute Error
0.0	0.000000	3.126830×10^{-9}	3.126830×10^{-9}
0.1	0.096140	0.096140	6.091750×10^{-8}
0.2	0.185994	0.185094	2.502260×10^{-7}
0.3	0.277724	0.267724	5.615220×10^{-7}
0.4	0.344936	0.344935	9.907840×10^{-7}
0.5	0.417640	0.417639	1.529500×10^{-6}
0.6	0.486722	0.486720	2.889860×10^{-6}
0.7	0.553026	0.553023	2.167090×10^{-6}
0.8	0.617343	0.617339	3.680790×10^{-6}
0.9	0.680401	0.680396	4.519730×10^{-6}
1.0	0.742860	0.742855	5.384880×10^{-6}

Table 3. The Comparison of HAM and ND-Solve for velocity function $g(\eta)$ w.r.t different values of the dimensionless variable η.

η	HAM Solution	ND Solution	Absolute Error
0.0	1.000000	1.000000	2.768567×10^{-8}
0.1	0.891532	0. 891533	7.671790×10^{-7}
0.2	0.803873	0. 803874	1.483510×10^{-6}
0.3	0.732482	0. 732484	2.160850×10^{-6}
0.4	0.674149	0. 674152	2.768330×10^{-6}
0.5	0.626630	0. 626634	3.297270×10^{-6}
0.6	0.588423	0. 588427	3.731420×10^{-6}
0.7	0.558623	0. 558627	2.062710×10^{-6}
0.8	0.536846	0. 536850	4.284390×10^{-6}
0.9	0.523221	0. 523225	4.404990×10^{-6}
1.0	0.518424	0. 518428	4.433930×10^{-6}

Table 4. Comparison of HAM and ND-Solve for temperature function $\theta(\eta)$ w.r.t. different values of the dimensionless variable η.

η	HAM Solution	ND Solution	Absolute Error
0.0	1.000000	1.000000	2.768560×10^{-8}
0.1	0.891532	0.891533	7.671790×10^{-6}
0.2	0. 803873	0.803884	1.483580×10^{-6}
0.3	0.732482	0.732484	2.160850×10^{-6}
0.4	0.674149	0.674152	2.768330×10^{-6}
0.5	0. 626630	0.626634	3.297270×10^{-6}
0.6	0.588423	0.588424	3.731420×10^{-6}
0.7	0.558623	0.558626	4.062710×10^{-6}
0.8	0.536846	0.536850	4.284390×10^{-6}
0.9	0. 523221	0.523225	4.404990×10^{-6}
1.0	0.518424	0.518428	4.439330×10^{-6}

Table 5. Individual residual square errors for Δ_m^f, Δ_m^g, Δ_m^θ.

Order↓	Values→	Δ_m^f	Δ_m^g	Δ_m^θ
4		0.0103907	0.00912399	6.0483×10^{-6}
8		0.0001435	0.0000458563	0.000012574
12		1.34066×10^{-6}	0.0000114474	5.85501×10^{-7}
16		2.48834×10^{-7}	2.51255×10^{-6}	7.2275×10^{-9}
20		1.0237×10^{-7}	1.42143×10^{-7}	2.17901×10^{-9}
24		9.63577×10^{-9}	3.28097×10^{-10}	1.09873×10^{-9}
30		7.35454×10^{-10}	1.38141×10^{-10}	4.68332×10^{-11}

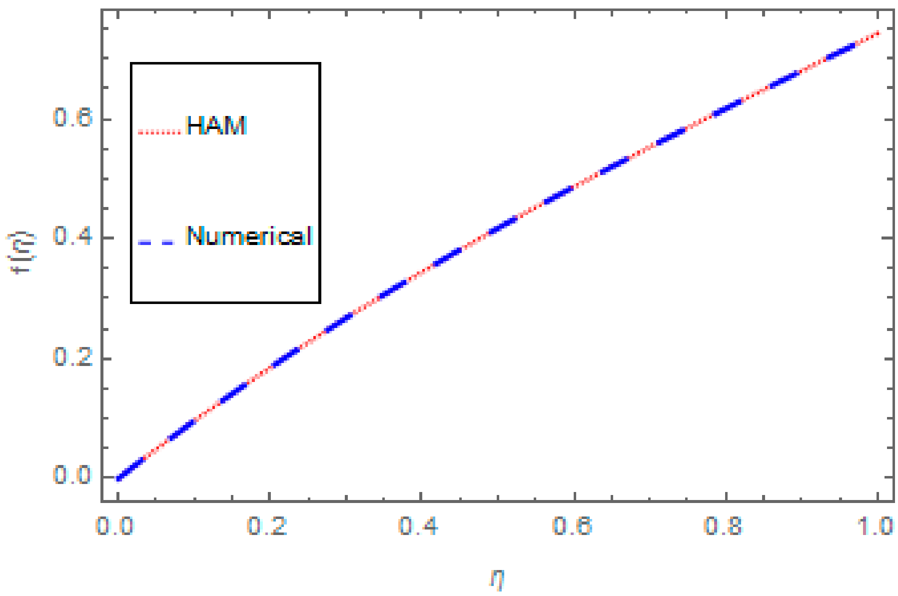

Figure 2. Comparison of the HAM and ND-Solve technique for velocity function $f(\eta)$.

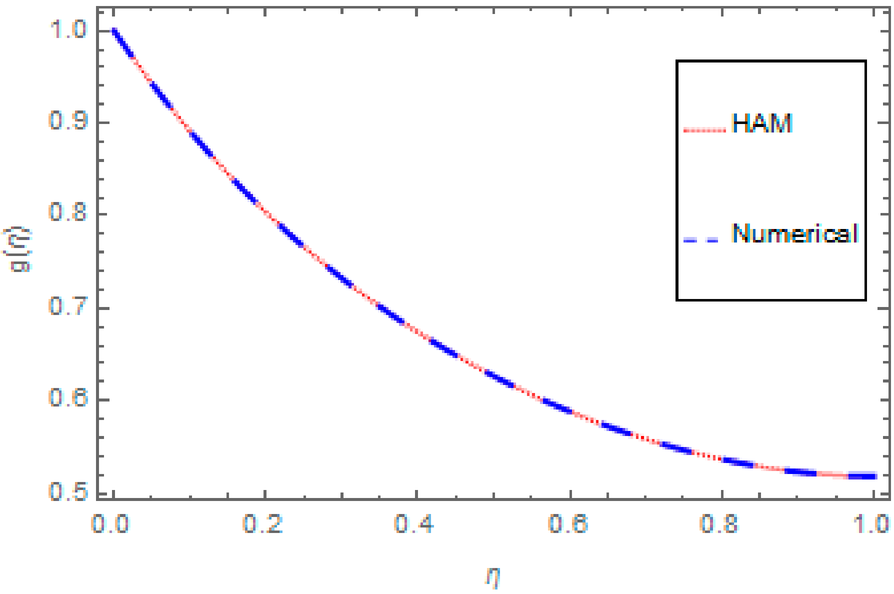

Figure 3. Comparison of the HAM and ND-Solve technique for velocity function $g(\eta)$.

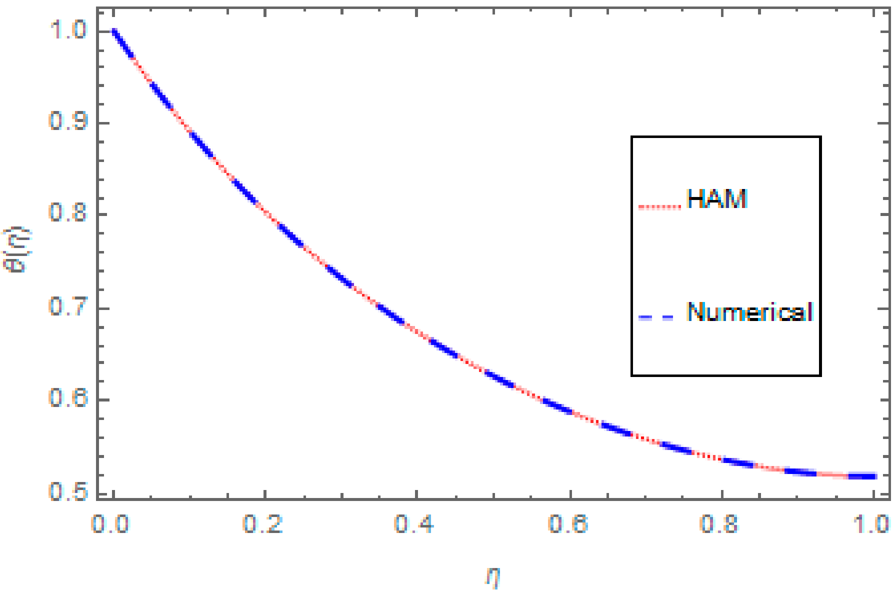

Figure 4. Comparison of the HAM and ND-Solve technique for temperature function $\theta(\eta)$.

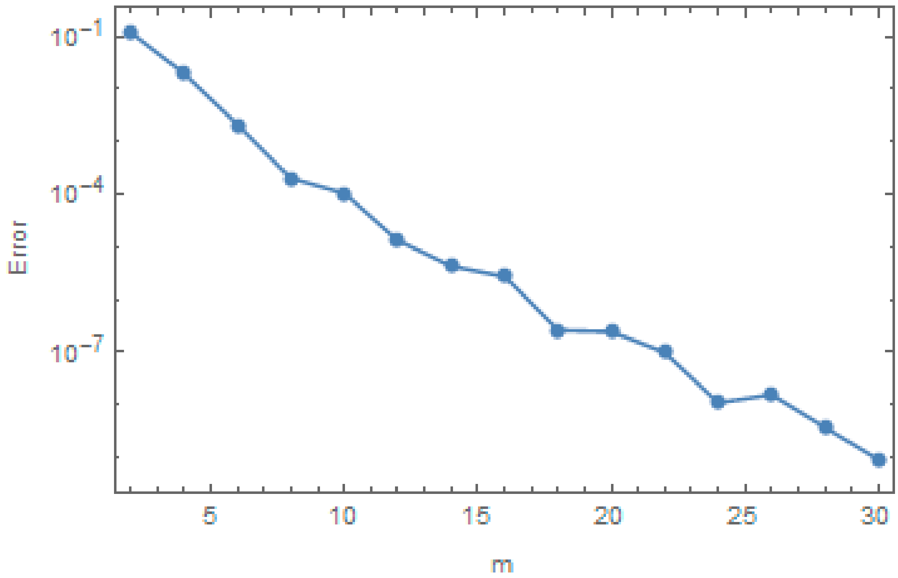

Figure 5. Residual Error.

4. Results and Discussion

In this section, we have presented Figures 6–16 to observe the impact of different embedded parameters on axial velocity $f(\eta)$, radial velocity $f'(\eta)$, and azimuthal velocity $g(\eta)$ and temperature $\theta(\eta)$ profiles. These parameters are unsteadiness (S), magnetic (M), Prandtl number (Pr), thermal radiation (Rd), temperature ratio (θ_w) of axial velocity $f(\eta)$, radial velocity $f'(\eta)$, azimuthal velocity $g(\eta)$ and temperature $\theta(\eta)$ profiles for some designated values. The effect of (M) on $f(\eta)$, $f'(\eta)$ and $g(\eta)$ is displayed in Figures 6–8. We observed a decaying trend in velocity components. The reason behind this is that the Lorentz force generated by the application of the axial magnetic field liquid opposes the liquid motion. A fan like behavior shows a rotating disk, which actually draws the fluid axially inward from the surrounding towards the disk surface. The inward fluid is rotated and releases in a radial direction because of the non-porous disk. Here the magnetic field is not applied directly, but is applied in the vertical direction, which slows down the axial flow. However, the magnetic force radial component slows down the motion in radial direction. The subsequent decrease in radial velocity causes the decrease in axial velocity. Moreover, the thickness is found in a decreasing fashion with the magnetic field parameter. Figures 9–12 are schemed to observe the influence of (S) on $f(\eta)$, $f'(\eta)$, $g(\eta)$ and $\theta(\eta)$. We observed that the growing (S) shows reducing behavior in $f(\eta)$, $f'(\eta)$, $g(\eta)$ and $\theta(\eta)$. Figure 13 shows the influence of (M) on $\theta(\eta)$. According to the Lorentz theory, the applied magnetic field reduces the thickness of the boundary layer flow and enhances the temperature of the fluid. Therefore, the increasing (M) enhances $\theta(\eta)$. Figure 14 illustrates the effect of (Rd) on $\theta(\eta)$. Physically, the escalating values of thermal radiation provide more heat to the liquid and as a result the growing temperature distribution arises inside the boundary layer thickness. From the sketch, we could see increasing behavior in the temperature profile with rising values of thermal radiation. Figure 15 shows the impact of (Pr) on $\theta(\eta)$. We could see increasing behavior in the temperature profile with the rise in Prandtl number. Figure 16 illustrates the influence of (θ_w) on $\theta(\eta)$. Physically, the strengthen temperature ratio parameter increases the wall temperature more than the ambient fluid temperature and as a result the fluid temperature upsurges. Therefore, $\theta(\eta)$ increases with the enhancement in (θ_w).

The relationship between the surface drag force and embedded parameters is presented in Table 6. The surface drag force diminishes with the augmentation in the magnetic field and the unsteadiness parameter. Similarly, the relationship between the heat transfer rate and embedded parameters is obtainable from Table 7. The heat transfer rate rises with the enhancement in the Prandtl number and the unsteadiness parameter.

Table 6. The numerical values for surface force w.r.t. different parameters.

M	S	Cf_r
0.1		−0.384263
0.2		−0.480181
0.3		−0.571465
	0.1	−0.518415
	0.2	−0.581053
	0.3	−0.640981

Table 7. The numerical values for heat transfer rate w.r.t. different parameters.

Rd	Pr	θ_w	S	Nu_r
0.1				0.970812
0.2				0.756927
0.3				0.632256
	5.0			0.237658
	5.5			0.657864
	6.0			0.987797
		0.1		0.161696
		0.2		0.161423
		0.3		0.160691
			0.1	0.208260
			0.2	0.234106
			0.3	0.259610

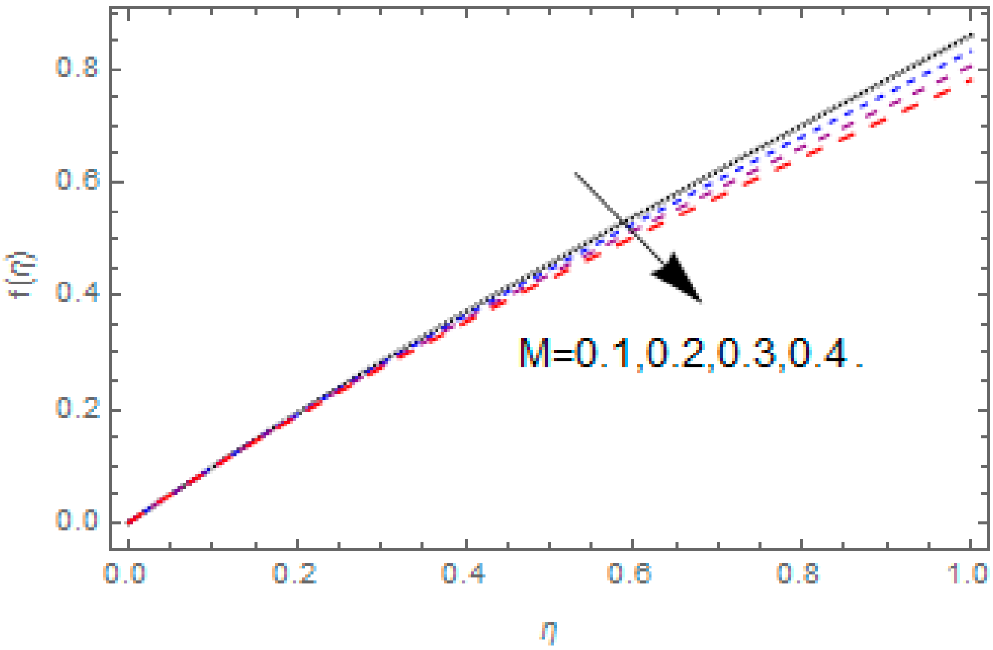

Figure 6. Influence of (M) on $f(\eta)$.

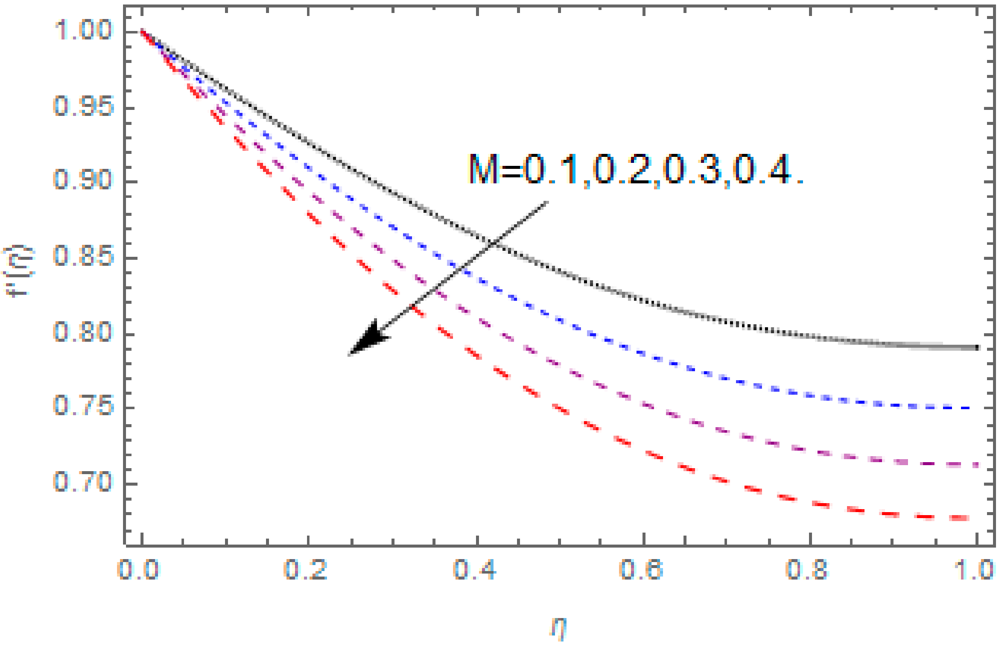

Figure 7. Influence of (M) on $f'(\eta)$.

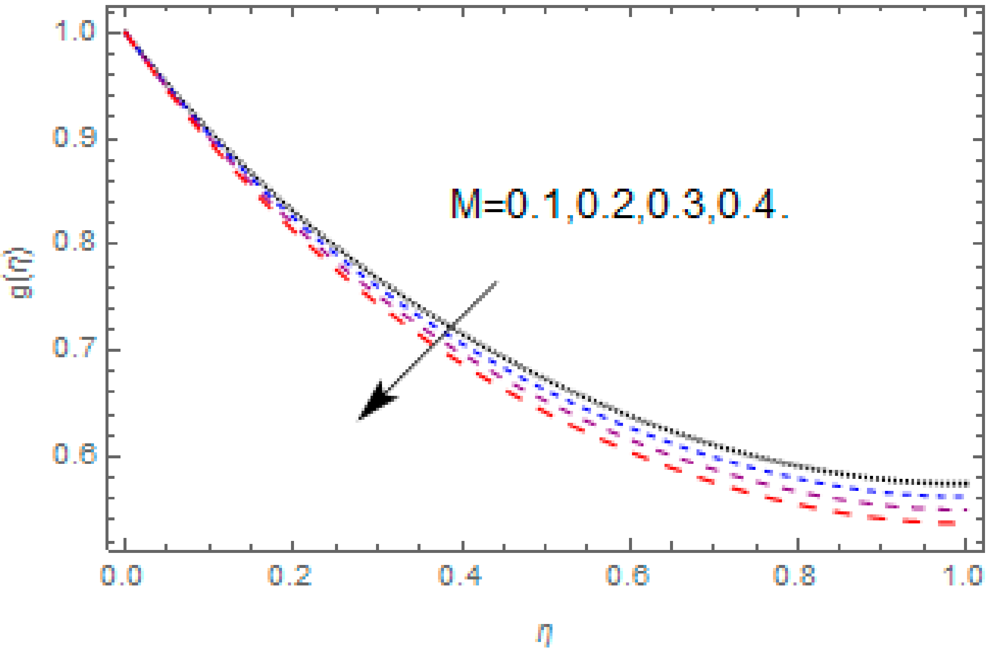

Figure 8. Influence of (M) on $g(\eta)$.

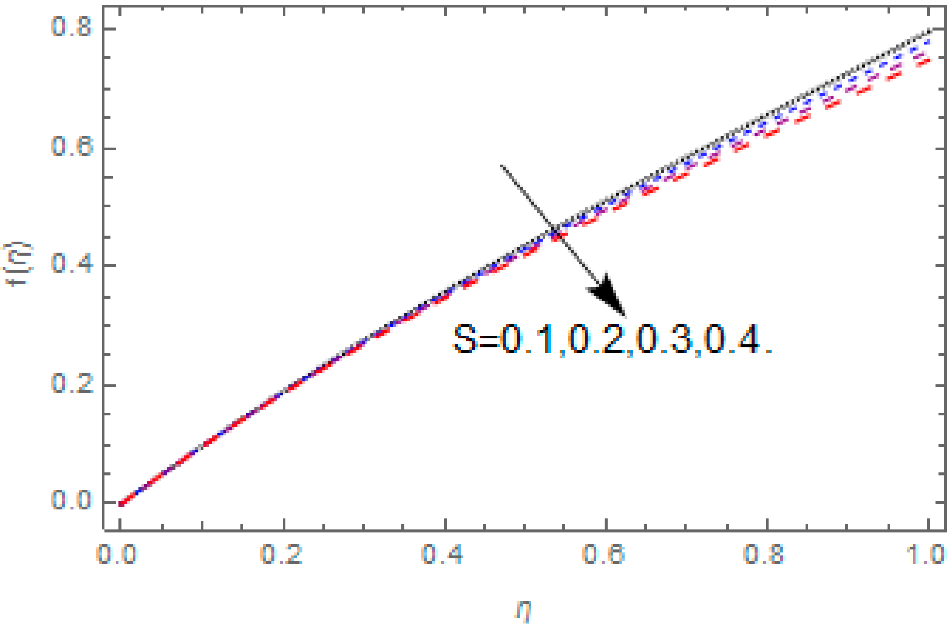

Figure 9. Influence of (S) on $f(\eta)$.

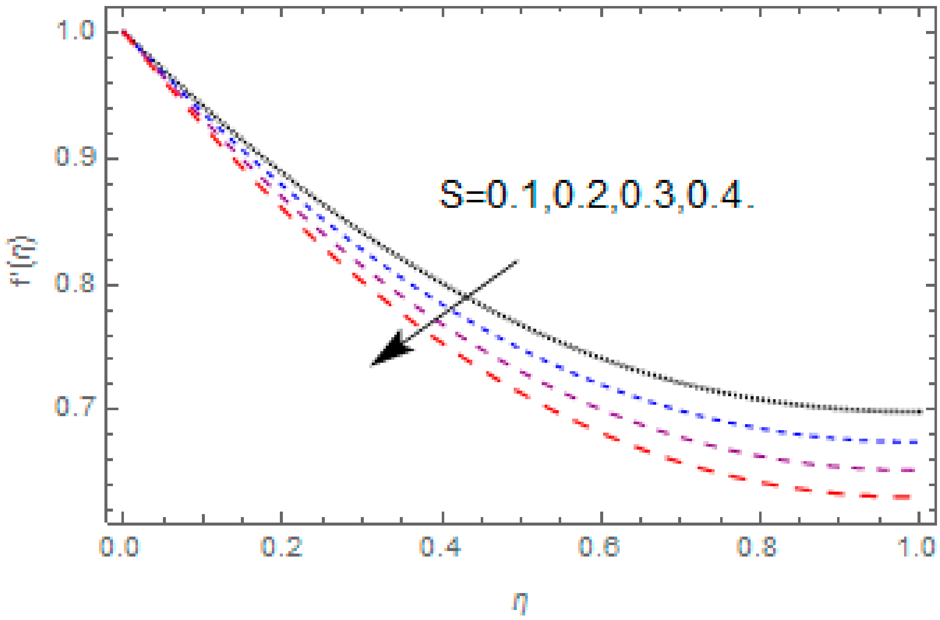

Figure 10. Influence of (S) on $f'(\eta)$.

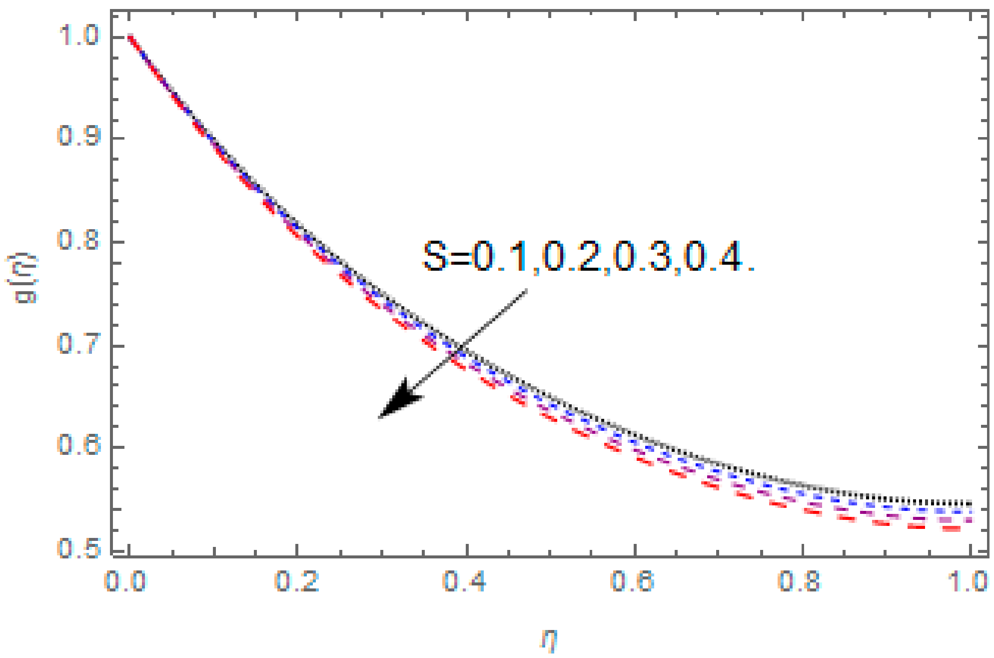

Figure 11. Influence of $\theta(\eta)$ on $g(\eta)$.

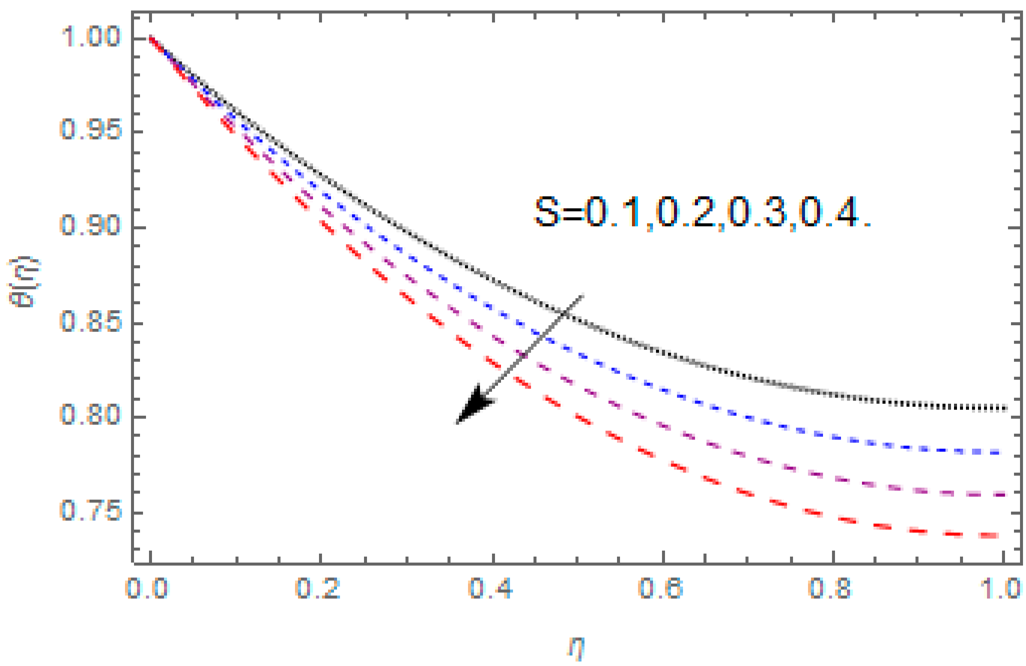

Figure 12. Influence of (S) on $\theta(\eta)$.

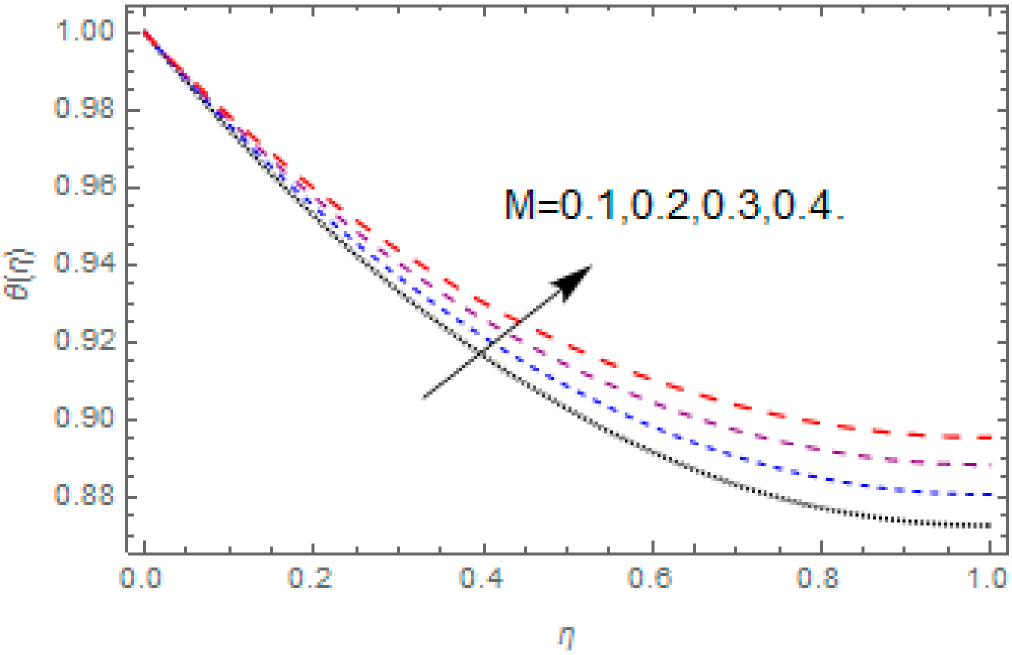

Figure 13. Influence of (M) on $\theta(\eta)$.

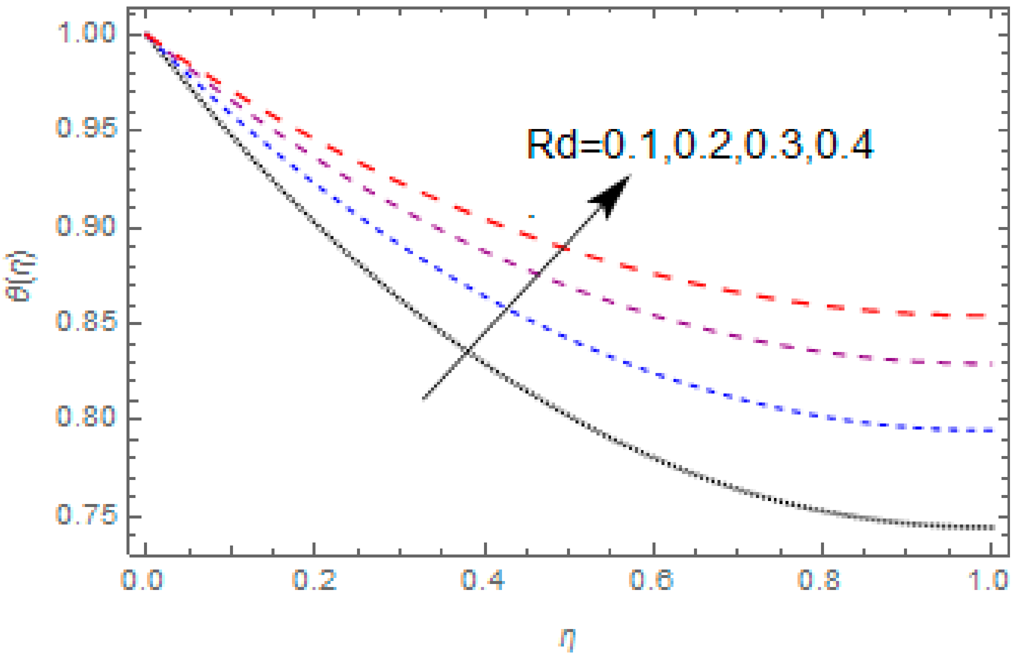

Figure 14. Influence of (Rd) on $\theta(\eta)$.

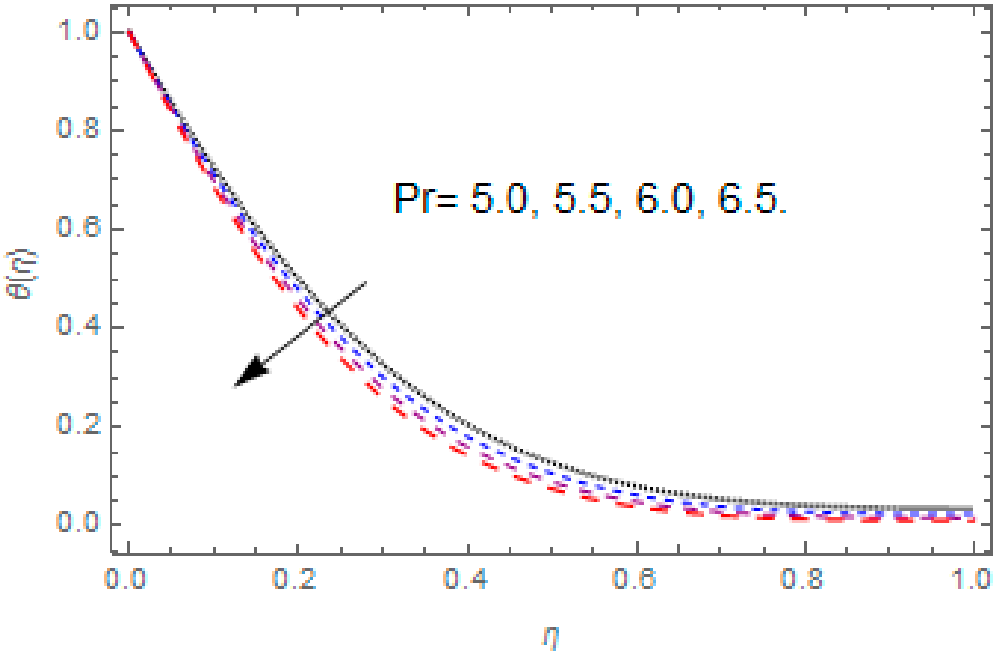

Figure 15. Influence of (Pr) on $\theta(\eta)$.

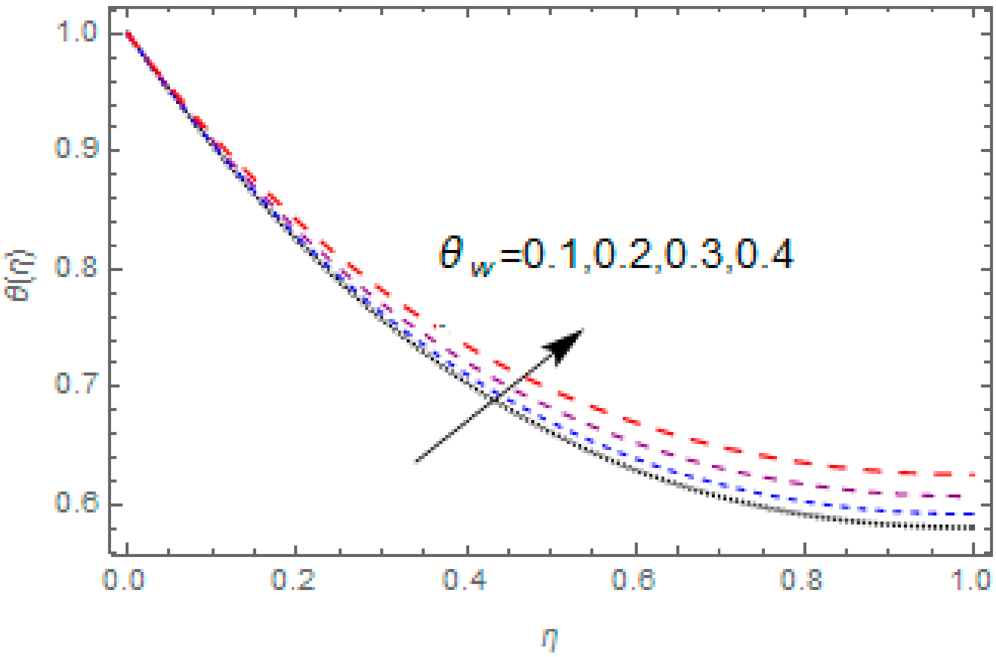

Figure 16. Influence of (θ_w) on $\theta(\eta)$.

5. Conclusions

In this article we have examined the unsteady flow of viscous fluid over a horizontally rotating disk. The impact of non-linear thermal radiations was studied numerically. The impact of the magnetic field has been taken into account. The theme of this article is listed below:

- The velocity profile reduced due to the escalated magnetic field.
- The temperature profile increased due to the escalated magnetic field.
- The velocity and temperature profiles raised due to the enhanced unsteadiness parameter.

- The temperature profile increased due to the enhanced temperature ration and thermal radiation parameters.
- The temperature profile reduced due to the enhanced Prandtl number.
- The skin fraction reduced due to the enhanced magnetic field and unsteadiness parameter.
- The local Nusselt number enhanced due to the enhanced Prandtl number and unsteadiness parameter.
- The local Nussetl number reduced due to the enhanced thermal radiation and temperature ratio parameters.

Author Contributions: Z.S. and A.D. modeled the problem and wrote the manuscript. P.K. and S.I. thoroughly checked the mathematical modeling and English corrections. W.K. and Z.S. solved the problem using Mathematica software. S.I. and P.K. contributed to the results and discussions. All authors finalized the manuscript after its internal evaluation.

Funding: This research was funded by the Center of Excellence in Theoretical and Computational Science (TaCS-CoE), KMUTT.

Acknowledgments: This project was supported by the Theoretical and Computational Science (TaCS) Center under Computational and Applied Science for Smart Innovation Research Cluster (CLASSIC), Faculty of Science, KMUTT.

Conflicts of Interest: The author declares that they have no competing interest.

Nomenclature

(r, φ, z)	cylindrical coordinate system
b	positive constant
T_s	Stretchable rotating disk surface temperature
T_{ref}	Constant reference temperature
$B(t)$	applied along z-direction
C_{ref}	reference concentration
u, v and w	velocity components
k^*	mean absorption coefficient
$\left(\rho C_p\right)_{nf}$	heat capacity
ρ_{nf}	Density
θ_w	temperature ratio parameter
Rd	radiation parameter
β	similarity variable at free space
c	stretching parameter
Ω	rotating rate of disk
T_0	Temperature at the origin
C_0	concentration at the origin
C_s	concentration at the disk surface
σ_{nf}	electrical conductivity
σ^*	Stephan–Boltzmann constant
ν_{nf}	kinematic viscosity
α_{nf}	thermal diffusivity
S	measure of unsteadiness
Pr	Prandtl number
ω	rotation parameter
M	magnetic parameter

References

1. Emslie, A.C.; Bonner, F.D.; Peck, L.G. Flow of a viscous liquid on a rotating disk. *J. Appl. Phys.* **1958**, *29*, 858–862. [CrossRef]
2. Higgins, B.G. Film flow on a rotating disk. *Phys. Fluids* **1986**, *29*, 3522. [CrossRef]

3. Dorfman, I.A. Flow and heat transfer in a.lm of viscous liquid on a rotating disk. *J. Eng. Phys.* **1967**, *12*, 162–166. [CrossRef]
4. Wang, C.Y.; Watson, L.T.; Alexander, K.A. Spinning of a liquid film from an accelerating disc. *IMA J. Appl. Math.* **1991**, *46*, 201–210. [CrossRef]
5. Andersson, H.I.; Holmedal, B.; Dandapat, B.S.; Gupta, A.S. Magnetohydrodynamic melting flow from a horizontal rotating disk. *Math. Models Methods Appl. Sci.* **1993**, *3*, 373–393. [CrossRef]
6. Dandapat, B.S.; Singh, S.K. Unsteady two-layer film flow on a non-uniform rotating disk in presence of uniform transverse magnetic field. *Appl. Math. Comput.* **2015**, *258*, 545–555. [CrossRef]
7. Sandeep, N.; Malvandi, A. Enhanced heat transfer in liquid thin film flow of non-Newtonian nanofluids embedded with graphene nanoparticles. *Adv. Powder Technol.* **2016**, *27*, 2448–2456. [CrossRef]
8. Usha, R.; Sridharan, R. On the motion of a liquid film on an unsteady stretching surface. *ASME Fluids Eng.* **1993**, *150*, 43–48. [CrossRef]
9. Khan, N.; Zuhra, S.; Shah, Z.; Bonyah, E.; Khan, W.; Islam, S. Slip flow of Eyring-Powell nanoliquid film containing graphene nanoparticles. *AIP Adv.* **2018**, *8*, 115302. [CrossRef]
10. Ullah, A.; Alzahrani, E.O.; Shah, Z.; Ayaz, M.; Islam, S. Nanofluids Thin Film Flow of Reiner-Philippoff Fluid over an Unstable Stretching Surface with Brownian Motion and Thermophoresis Effects. *Coatings* **2019**, *9*, 21. [CrossRef]
11. Shah, Z.; Bonyah, E.; Islam, S.; Khan, W.; Ishaq, M. Radiative MHD thin film flow of Williamson fluid over an unsteady permeable stretching. *Heliyon* **2018**, *4*, e00825. [CrossRef] [PubMed]
12. Ishaq, M.; Ali, G.; Shah, S.I.A.; Shah, Z.; Muhammad, S.; Hussain, S.A. Nanofluid Film Flow of Eyring Powell Fluid with Magneto Hydrodynamic Effect on Unsteady Porous Stretching Sheet. *Punjab Univ. J. Math.* **2019**, *51*, 131–153.
13. Jawad, M.; Shah, Z.; Islam, S.; Islam, S.; Bonyah, E.; Khan, Z.A. Darcy-Forchheimer flow of MHD nanofluid thin film flow with Joule dissipation and Navier's partial slip. *J. Phys. Commun.* **2018**. [CrossRef]
14. Jawad, M.; Shah, Z.; Islam, S.; Majdoubi, J.; Tlili, I.; Khan, W.; Khan, I. Impact of Nonlinear Thermal Radiation and the Viscous Dissipation Effect on the Unsteady Three-Dimensional Rotating Flow of Single-Wall Carbon Nanotubes with Aqueous Suspensions. *Symmetry* **2019**, *11*, 207. [CrossRef]
15. Megahe, A.M. Effect of slip velocity on Casson thin film flow and heat transfer due to unsteady stretching sheet in presence of variable heat flux and viscous dissipation. *Appl. Math. Mech. Engl. Ed.* **2015**, *36*, 1273–1284. [CrossRef]
16. Khan, N.S.; Gul, T.; Islam, S.; Khan, A.; Shah, Z. Brownian Motion and Thermophoresis Effects on MHD Mixed Convective Thin Film Second-Grade Nanofluid Flow with Hall Effect and Heat Transfer Past a Stretching Sheet. *J. Nanofluids* **2017**, *6*, 1–18. [CrossRef]
17. Tahir, F.; Gul, T.; Islam, S.; Shah, Z.; Khan, A.; Khan, W.; Ali, L.; Muradullah. Flow of a Nano-Liquid Film of Maxwell Fluid with Thermal Radiation and Magneto Hydrodynamic Properties on an Unstable Stretching Sheet. *J. Nanofluids* **2017**, *6*, 1021–1030. [CrossRef]
18. Sheikholeslami, M.; Shah, Z.; Tassaddiq, A.; Shafee, A.; Khan, I. Application of Electric Field for Augmentation of Ferrofluid Heat Transfer in an Enclosure Including Double Moving Walls. *IEEE Access* **2019**, *7*, 21048–21056. [CrossRef]
19. Sheikholeslami, M.; Gerdroodbary, M.B.; Moradi, R.; Shafee, A.; Zhixiong, L. Application of Neural Network for estimation of heat transfer treatment of Al_2O_3-H_2O nanofluid through a channel. *Comput. Methods Appl. Mech. Eng.* **2019**, *344*, 1–12. [CrossRef]
20. Sheikholeslami, M.; Mehryan, S.A.M.; Shafee, A.; Sheremet, M.A. Variable magnetic forces impact on Magnetizable hybrid nanofluid heat transfer through a circular cavity. *J. Mol. Liq.* **2019**, *277*, 388–396. [CrossRef]
21. Sheikholeslami, M.; Shah, Z.; Shafi, A.; khan, I.; Itili, I. Uniform magnetic force impact on water based nanofluid thermal behavior in a porous enclosure with ellipse shaped obstacle. *Sci. Rep.* **2019**. [CrossRef]
22. Malik, M.Y.; Khan, I.; Hussain, A.; Salahuddin, T. Mixed convection flow of MHD Erying-Powell nanofluid over a stretching sheet: A numerical study. *AIP Adv.* **2015**, *5*, 117–118. [CrossRef]
23. Nadeem, S.; Haq, R.U.; Khan, Z.H. Numerical study of MHD boundary layer flow of a Maxwell fluid past a stretching sheet in the presence of nanoparticles. *J. Taiwan Inst. Chem. Eng.* **2014**, *45*, 121–126. [CrossRef]

24. Raju, C.S.K.; Sandeep, N.; Malvandi, A. Free convective heat and mass transfer of MHD non-Newtonian nanofluids over a cone in the presence of non-uniform heat source/sink. *J. Mol. Liq.* **2016**, *221*, 108–115. [CrossRef]
25. Rokni, H.B.; Alsaad, D.M.; Valipour, P. Electrohydrodynamic nanofluid flow and heat transfer between two plates. *J. Mol. Liq.* **2016**, *216*, 583–589. [CrossRef]
26. Nadeem, S.; Rizwan, U.H.; Khan, Z.H. Numerical solution of non-Newtonian nanofluid flow over a stretching sheet. *Appl. Nanosci.* **2014**, *5*, 625–631. [CrossRef]
27. Shehzad, S.A.; Hayat, T.; Alsaedi, A. MHD flow of Jeffrey nanofluid with convective boundary conditions. *Braz. Soc. Mech. Sci. Eng.* **2014**, *3*, 873–883. [CrossRef]
28. Sheikholeslami, M.; Hatami, H.M.; Ganji, D.D. Nanofluid flow and heat transfer in a rotating system in the presence of a magnetic field. *J. Mol. Liq.* **2014**, *190*, 112–120. [CrossRef]
29. Shah, Z.; Islam, S.; Ayaz, H.; Khan, S. Radiative Heat and Mass Transfer Analysis of Micropolar Nanofluid Flow of Casson Fluid between Two Rotating Parallel Plates with Effects of Hall Current. *ASME J. Heat Transf.* **2019**. [CrossRef]
30. Shah, Z.; Islam, S.; Gul, T.; Bonyah, E.; Altaf Khan, M. The elcerical MHD and hall current impact on micropolar nanofluid flow between rotating parallel Plates. *Results Phys.* **2018**. [CrossRef]
31. Shah, Z.; Dawar, A.; Islam, S.; Khan, I.; Ching, D.L.C. Darcy-Forchheimer Flow of Radiative Carbon Nanotubes with Microstructure and Inertial Characteristics in the Rotating Frame. *Case Stud. Therm. Eng.* **2018**, *12*, 823–832. [CrossRef]
32. Shah, Z.; Bonyah, E.; Islam, S.; Gul, T. Impact of thermal radiation on electrical mhd rotating flow of carbon nanotubes over a stretching sheet. *AIP Adv.* **2019**, *9*, 015115. [CrossRef]
33. Shah, Z.; Dawar, A.; Islam, S.; Khan, I.; Ching, D.L.C.; Khan, A.Z. Cattaneo-Christov model for Electrical MagnetiteMicropoler Casson Ferrofluid over a stretching/shrinking sheet using effective thermal conductivity model. *Case Stud. Therm. Eng.* **2018**. [CrossRef]
34. Shah, Z.; Tassaddiq, A.; Islam, S.; Alklaibi, A.; Khan, I. Cattaneo–Christov Heat Flux Model for Three-Dimensional Rotating Flow of SWCNT and MWCNT Nanofluid with Darcy–Forchheimer Porous Medium Induced by a Linearly Stretchable Surface. *Symmetry* **2019**, *11*, 331. [CrossRef]
35. Hammed, K.; Haneef, M.; Shah, Z.; Islam, I.; Khan, W.; Asif, S.M. The Combined Magneto hydrodynamic and electric field effect on an unsteady Maxwell nanofluid Flow over a Stretching Surface under the Influence of Variable Heat and Thermal Radiation. *Appl. Sci.* **2018**, *8*, 160. [CrossRef]
36. Dawar, A.; Shah, Z.; Khan, W.; Idrees, M.; Islam, S. Unsteady squeezing flow of MHD CNTS nanofluid in rotating channels with Entropy generation and viscous Dissipation. *Adv. Mech. Eng.* **2019**, *10*, 1–18. [CrossRef]
37. Khan, A.S.; Nie, Y.; Shah, Z.; Dawar, A.; Khan, W.; Islam, S. Three-Dimensional Nanofluid Flow with Heat and Mass Transfer Analysis over a Linear Stretching Surface with Convective Boundary Conditions. *Appl. Sci.* **2018**, *8*, 2244. [CrossRef]
38. Dzulkifli, N.F.; Bachok, N.; Yacob, N.A.; Md Arifin, N.; Rosali, H. Unsteady Stagnation-Point Flow and Heat Transfer Over a Permeable Exponential Stretching/Shrinking Sheet in Nanofluid with Slip Velocity Effect: A Stability Analysis. *Appl. Sci.* **2018**, *8*, 2172. [CrossRef]
39. Mahian, O.; Kolsi, L.; Amani, M.; Estellé, P.; Ahmadi, G.; Kleinstreuer, C.; Marshall, S.J.; Taylor, R.A.; Abu-Nada, E.; Rashidi, S.; et al. Recent advances in modeling and simulation of nanofluid flows—Part II: Applications. *Phys. Rep.* **2019**, *791*, 1–59. [CrossRef]
40. Mahian, O.; Kolsi, L.; Amani, M.; Estellé, P.; Ahmadi, G.; Kleinstreuer, C.; Marshall, S.J.; Taylor, R.A.; Abu-Nada, E.; Rashidi, S.; et al. Recent advances in modeling and simulation of nanofluid flows-Part I: Fundamentals and theory. *Phys. Rep.* **2019**, *790*, 1–48. [CrossRef]
41. Vo, D.; Alsarraf, J.; Moradikazerouni, A.; Afrand, M.; Salehipour, H.; Qi, K. Numerical investigation of γ-AlOOH nano-fluid convection performance in a wavy channel considering various shapes of nanoadditives. *Powder Technol.* **2019**, *345*, 649–657. [CrossRef]
42. Moradikazerouni, A.; Hajizadeh, A.; Safae, M.R.; Afrand, M.; Yarmand, H.; Zulkifli, N.W.B.M. Assessment of thermal conductivity enhancement of nano-antifreeze containing single-walled carbon nanotubes: Optimal artificial neural network and curve-fitting. *Phys. A Stat. Mech. Its Appl.* **2019**, *521*, 138–145. [CrossRef]

43. Alsarraf, J.; Moradikazerouni, A.; Afrand, M.; Shahsavar, A.; Salehipour, H.; Tran, M.D. Hydrothermal analysis of turbulent boehmite alumina nanofluid flow with different nanoparticle shapes in a minichannel heat exchanger using two-phase mixture model. *Phys. A Stat. Mech. Its Appl.* **2019**, *520*, 275–288. [CrossRef]
44. Nasir, S.; Shah, Z.; Islam, S.; Khan, W.; Khan, S.N. Radiative flow of magneto hydrodynamics single-walled carbon nanotube over a convectively heated stretchable rotating disk with velocity slip effect. *Adv. Mech. Eng.* **2019**, *11*, 1–11. [CrossRef]
45. Nasir, S.; Shah, Z.; Islam, S.; Khan, W.; Bonyah, E.; Ayaz, M.; Khan, A. Three dimensional Darcy-Forchheimer radiated flow of single and multiwall carbon nanotubes over a rotating stretchable disk with convective heat generation and absorption. *AIP Adv.* **2019**, *9*, 035031. [CrossRef]
46. Khan, A.; Shah, Z.; Islam, S.; Dawar, A.; Bonyah, E.; Ullah, H.; Khan, Z.A. Darcy-Forchheimer flow of MHD CNTs nanofluid radiative thermal behaviour andconvective non uniform heat source/sink in the rotating frame with microstructureand inertial characteristics. *AIP Adv.* **2018**, *8*, 125024. [CrossRef]
47. Khan, A.; Shah, Z.; Islam, S.; Khan, S.; Khan, W.; Khan, Z.A. Darcy–Forchheimer flow of micropolar nanofluid between two plates in the rotating frame with non-uniform heat generation/absorption. *Adv. Mech. Eng.* **2018**, *10*, 1–16. [CrossRef]
48. Feroz, N.; Shah, Z.; Islam, S.; Alzahrani, E.O.; Khan, W. Entropy Generation of Carbon Nanotubes Flow in a Rotating Channel with Hall and Ion-Slip Effect Using Effective Thermal Conductivity Model. *Entropy* **2019**, *21*, 52. [CrossRef]
49. Alharbi, S.O.; Dawar, A.; Shah, Z.; Khan, W.; Idrees, M.; Islam, S.; Khan, I. Entropy Generation in MHD Eyring–Powell Fluid Flow over an Unsteady Oscillatory Porous Stretching Surface under the Impact of Thermal Radiation and Heat Source/Sink. *Appl. Sci.* **2018**, *8*, 2588. [CrossRef]
50. Muhammad, S.; Ali, G.; Shah, Z.; Islam, S.; Hussain, S.A. The Rotating Flow of Magneto Hydrodynamic Carbon Nanotubes over a Stretching Sheet with the Impact of Non-Linear Thermal Radiation and Heat Generation/Absorption. *Appl. Sci.* **2018**, *8*, 482. [CrossRef]